# Role of Structural Defects in the Water Adsorption Properties of MOF-801

Jongwon Choi,[†] Li-Chiang Lin,[‡,*] and Jeffrey C. Grossman[†,*]

[†]Department of Materials Science and Engineering, Massachusetts Institute of Technology, Cambridge, Massachusetts 02139, United States

[‡]William G. Lowrie Department of Chemical and Biomolecular Engineering, The Ohio State University, Columbus, Ohio 43210, United States

S Supporting Information

ABSTRACT: The nanoporous and tunable nature of metal–organic frameworks (MOFs) has made them promising adsorbents for water adsorption applications such as water harvesting and adsorptive heat pumps. In these applications, water adsorption properties in MOFs play a crucial role. However, understanding their structural defects and how defects influence adsorption thermodynamics remains limited to date. In this work, by employing Monte Carlo techniques and first-principle density functional theory calculations, we investigate the effect of defects on the water adsorption properties in MOF-801 structures at an atomic level. Our calculations show that the adsorption isotherm in perfect MOF-801 (without defects) greatly deviates from that measured experimentally. With the introduction of defects with a high density,

a reasonably good agreement can be achieved, suggesting that a high defect density in MOF-801 may be responsible for its hydrophilic adsorptive behaviors. Further, water adsorption properties in MOF-801 structures are found to depend on the spatial configuration of defects, and water condensation in nanoporous MOF-801 is identified to occur preferentially along the ⟨110⟩ direction. Detailed structural characteristics (accessible volume, etc.) of MOF-801 structures and the adsorption energetics of water in the frameworks are also studied and correlated with the computed adsorption isotherms. Our findings reveal important insights into the role of defects, offering a microscopic picture to help facilitate the rational design of better MOFs for water adsorption applications.
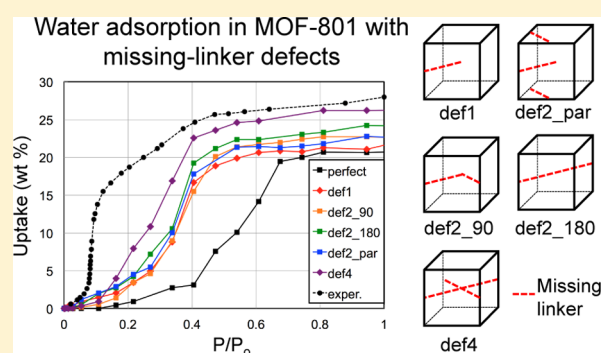
INTRODUCTION

Metal–organic frameworks (MOFs) are an emerging class of crystalline nanoporous materials that have received considerable attention over the past decade.[1–4] Their controllable pore structures,[5] exceptionally high surface area,[6,7] and decent thermal and chemical robustness[5] have made them promising candidates as adsorbents for a variety of energy- and environment-related applications.[5–10] Specifically, among a wide range of possible guest molecules that have been studied for their adsorption properties in MOFs, water adsorption in MOFs has received particular attention recently for water-harvesting and heat transformation applications.[11–15] A recent experimental study reported that 1 kg of MOF-801 is capable of capturing 2.8 L of water daily from ambient air at a low relative humidity level (~20%) without any additional energy input.[11] MOFs have also been proposed as adsorbents for heat transformation applications, that is, heat pumps, thermal storage, and/or refrigeration[12–15] because of the large heats of adsorption together with high adsorption capacity.[16] As attention around water adsorption applications using MOFs continues to grow, an improved atomic-level understanding regarding the water adsorption properties in MOFs is of critical

importance toward the continued rational design of MOFs with enhanced performance.

One important aspect of MOFs is their structural defects, which can be potentially exploited and designed to engineer materials properties and therefore enhance their performance in a given application.[17–19] Although using MOFs as water adsorbents has drawn increasing attention, understanding the effect of structural defects on their water adsorption properties remains limited. As an example, one of the most heavily studied water-stable MOFs, UiO-66, is prone to possess a high defect density of ~1/12 (i.e., two missing linkers per unit cell).[20–26] Although the presence of defects may not be ideal for the thermal and mechanical stability of MOFs,[21,24] it has been demonstrated both theoretically[27] and experimentally[26,28] that defects can increase the hydrophilicity of MOFs, leading to enhanced water adsorption properties. Yet, it remains generally unclear how the spatial configuration of defects will affect the water adsorption properties. In addition, little is known at the

microscopic level about the water adsorption process inside MOFs that contain defects. Accordingly, we aim to shed light on the effects of configuration and density of defects on the water adsorption properties. Specifically, we focus on MOF-801,[11,29,30] another water-stable MOF structure, that has been studied previously for its promising water-harvesting ability as introduced above. MOF-801 is a zirconium-based MOF with a chemical composition of $Zr_6O_4(OH)_4(fumarate)_6$ (i.e., in the absence of defects, denoted as perfect MOF-801 structures). MOF-801 may also possess defects as discussed in the work of Furukawa et al.[30] This is also reflected on the results of the elementary analysis, where the carbon and hydrogen element percentage of the synthesized samples after activation was found to be lower than that of perfect MOF-801 structures.[30] In this study, state-of-the-art Monte Carlo simulations in the grand canonical and canonical ensembles are employed to show that the water adsorption in MOFs occurs primarily near defect sites and with a growing number of defects, the MOF becomes more hydrophilic. This observation is supported by the calculated adsorption energetics (intermolecular interactions) of water with defective MOF structures. At a defect density of 1/6 (four missing linkers per unit cell in MOF-801), the simulated water adsorption isotherm resembles the experimentally reported[30] one reasonably well. Furthermore, a detailed investigation of the spatial arrangement of defects indicates its profound effect on the water adsorption behavior, and preferential water adsorption sites are observed in the ⟨110⟩ directions of the MOF-801 crystal. Depending on the defect configuration, the density of the adsorbed water phase in MOF-801 can vary considerably, which, in turn, affects the maximum adsorption capacity of the MOF structure.

■ COMPUTATIONAL DETAILS

In this study, a perfect MOF-801 crystal and five illustrative MOF-801 structures with different defect densities and/or configurations as shown in Figure 1 were systematically investigated. The particular type of defects focused herein is the missing-linker defects. We considered defect densities varying from 1/24, 1/12, to 1/6, corresponding to 1, 2, and 4
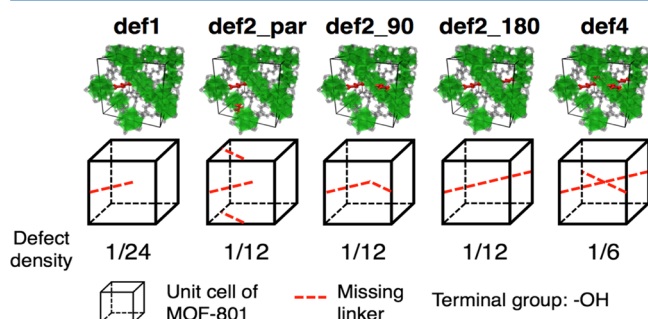

Figure 1. Five MOF-801 defect structures with different defect densities and/or spatial configurations are considered in this work. Green polyhedra represent the metal clusters, whereas missing linkers are highlighted in red. The relative position of the missing linkers is schematically illustrated in cubic boxes. The first number in the structure name indicates how many linkers were removed per unit cell (e.g., def2: a MOF-801 structure with two missing linkers per unit cell). Additionally, the notations after the underscore refer to different relative configurations of the defects (i.e., par: defects are perpendicular to each other and located in different planes, 90: defects are perpendicular to each other and located in the same plane, 180: defects are in parallel and located in the same plane).

missing linkers per unit cell, respectively (denoted also, respectively, as def1, def2, and def4). To obtain insights into the effects of spatial defect configurations on water adsorption properties, three structures with two missing linkers in different arrangements (i.e., def2_90, def2_180, and def_par, see Figure 1) were constructed and studied. We note that the particular def4 structure investigated in this work was built based upon an observation made from def2_180, where the clustering of water was found to be facilitated when linkers were removed along the ⟨110⟩ direction (see below for details). To further promote the condensation of water, two additional linkers were therefore removed along this direction, resulting in a highly symmetric def4 structure. For all of these structures with missing linkers, hydroxyl groups were attached to ensure charge neutrality. The atomic structures for all defect structures were relaxed using first-principle density functional theory (DFT) calculations implemented in the VASP software.[31−33] Projected augmented-wave pseudopotentials[34,35] were used with the generalized gradient approximation using the Perdew−Burke−Ernzerhof functional.[36,37] A plane-wave cutoff energy of 800 eV was used with a self-consistency convergence criterion of 10^{-4} eV and an ionic relaxation criterion of 10^{-3} eV/Å. As the unit cell is relatively large (i.e., ∼18 Å), single gamma-point DFT calculations were carried out. For simplicity, all MOF structures have the same cubic lattice with a cell length of 17.8348 Å in each direction as experimentally determined in the previous work.[30] The coordinate information of all structures and the corresponding unit cell formulas can be found in the Supporting Information.

Gas adsorption isotherms in MOFs were calculated using Monte Carlo within the grand canonical ensemble (i.e., GCMC simulations) as implemented in the RASPA package.[38] The interatomic interactions are described with 6-12 Lennard-Jones (L-J) and long-range Coulomb interactions. The L-J potentials were truncated and shifted to zero at a cutoff distance of 12 Å, whereas the long-range Coulomb interactions were computed using the Ewald summation technique.[39] The L-J parameters for the framework atoms were modeled using the DREIDING force field[40] except for the zirconium atoms whose parameters were instead from the universal force field (UFF).[41] The partial charges for the MOF atoms were determined by the REPEAT algorithm[42] using electrostatic potentials obtained from the aforementioned first-principle DFT calculations. Water molecules were described by the TIP4P-EW model.[43] In the calculations for each structure, a supercell comprising $2 \times 2 \times 2$ unit cells was used, ensuring the simulation box to be of at least twice the cutoff radius along each crystal direction. To compute P/P_0 in all the water isotherms presented in this study, the saturation pressure, P_0, is set to be 3750 Pa at room temperature,[44] according to the computed vapor pressure using the TIP4P-Ew model. The GCMC calculations were carried out for a pressure range of 1−3750 Pa at 298 K. NVT calculations (Monte Carlo simulations in the canonical ensemble) were also performed to investigate the interaction energies and water adsorption configurations of the system at a given adsorption loading. For these NVT simulations, initial configurations were adopted from snapshots of GCMC simulations.

■ RESULTS AND DISCUSSION

The computed water adsorption isotherms for perfect MOF-801 and MOF-801 with defects, along with the experimental data reported in the literature,[30] are summarized in Figure 2.
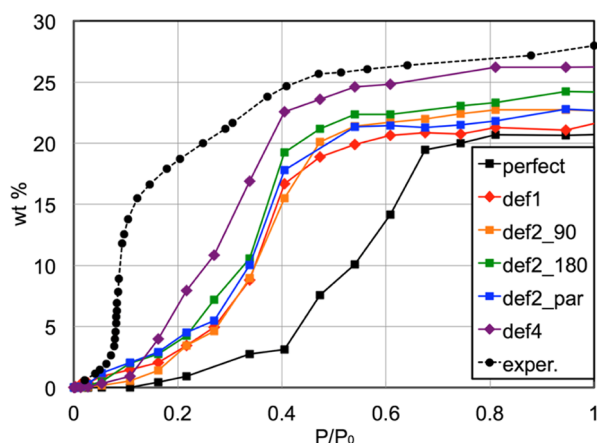
Figure 2. Water adsorption isotherms of perfect MOF-801 and defect structures. The solid lines represent the results obtained from the GCMC calculations, and the experimental measurement reported in the literature by Furukawa et al.[30] is plotted with a dashed line.

The calculated water isotherm in the perfect crystal shows a large deviation from the experimental measurement. A gradual increase in adsorption uptake starting at around 40% partial pressure was found in contrast to a sharp condensation at 6% relative pressure observed in experiments. Moreover, its maximum adsorption uptake value was calculated to be 26% smaller than that of the experimental value. The discrepancy between simulation predictions and experimental measurements is substantially reduced when defects are introduced, demonstrating that defects in MOF-801 indeed play a crucial role in its promising adsorption properties. As the number of defects increases, the maximum water adsorption uptake increases and the isotherm tends to shift to the left (i.e., stronger adsorption affinity to water) as shown in Figure 2, indicating a more hydrophilic nature. This also suggests that the characteristic of water adsorption isotherms in MOFs may be used to probe their structural defects, in agreement with that reported in the work of Dissegna et al.[26] Increase in hydrophilic behavior can be attributed to the interaction between water molecules and the hydroxyl groups attached onto metal nodes when defects are introduced. Although all studied MOFs with defects still appear to possess more hydrophobic characteristics with a lower uptake as compared to the experimentally determined isotherm, the simulated isotherm of MOF-801 with the highest density of defects (i.e., def4 that has a defect density of 1/6, representing four missing linkers per unit cell) is in decent agreement with the experimental one. A steep increase in the water adsorption of the def4 sample occurs at around 10% relative pressure and the uptake goes up to 92% of the experimental value at a high relative pressure. At this point, it is important to note that some uncertainties may be involved in the comparison between experimental measurements and our simulation results. First, experimental measurements of water isotherms have been known to be challenging because of, for example, inconsistencies of the structures from the synthesis process, the possibility of slow dynamics inside the framework, and difficulties in precise control over the vapor pressure.[45] As a specific example, the isotherm measurements of water adsorption in Mg-MOF-74, an open-metal-site MOF, reported in the literature show a wide range of uptake values.[45−48] Next, we have only considered one type of defects (i.e., missing linkers with hydroxyl terminals), whereas other forms of defects may possibly exist as well. For instance, it has been reported

that structural defects may also result in unsaturated metal sites.[49−51] With the presence of unsaturated metal sites, the adsorption strength of water at the low-pressure region may be substantially enhanced.[45] Additionally, no molecular potential has been specifically developed to date to model this particular system, and therefore, parameters from generic force fields including DREIDING[40] and UFF[41] were adopted in this study. It has been recently demonstrated that accurate force fields for describing gaseous adsorption in MOFs can be achieved by using ab initio calculations.[52−54] To accurately describe water molecules adsorbed onto MOFs, interaction energies between water and a variety of MOFs (such as MOF-74 and CuBTC) calculated by DFT have been used as references to parameterize potential parameters.[45,55−57] However, such a detailed potential development is out of the scope of this work and can be an important subject of future studies. Finally, the nature of water simulations in porous materials requires a considerable amount of time (i.e., calculations take several months), and it is therefore difficult to ensure that global equilibrium has been achieved. A recent study demonstrates that advanced Monte Carlo schemes such as continuous fractional component Monte Carlo[58] can notably speed up the calculations for water adsorption isotherms, which may potentially help address such difficulty.[59] Overall, considering all the aforementioned uncertainties, the qualitative agreement between simulations and experiments achieved herein can be considered quite good. For those samples with fewer defects (i.e., def1 and def2), their predicted isotherms exhibit some minor differences. Among the def2 samples, def2_180 shows the highest uptake, whereas def2_par and def2_90 samples show a comparable amount of uptake. The effects of density and spatial configuration of defects on adsorption thermodynamics are discussed in greater detail below.

The increased hydrophilicity with the presence of defects can be primarily attributed to the increased Coulomb interaction from the hydroxyl terminal group at the defect sites. Figure 3 compares the host−adsorbate (denoted as H−A between the adsorbed water molecules and the framework) interaction energy of the perfect MOF-801 and def1 structures as a function of adsorption uptake. For the perfect structure, the van der Waals (vdW) and Coulomb contributions of the H−A interaction are similar and remain relatively constant at uptakes
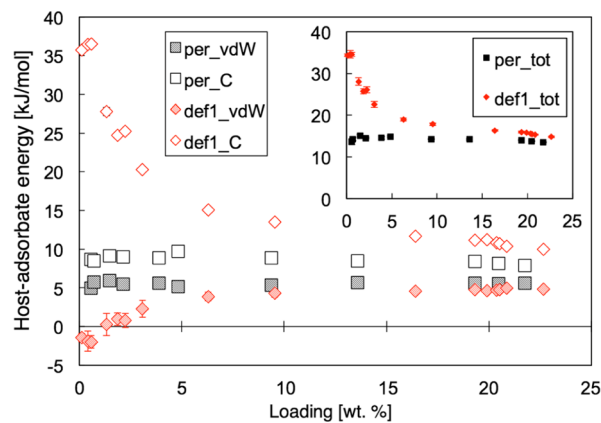
Figure 3. vdW and Coulomb contributions to the H−A energy of perfect and def1 structures. The inset displays the total H−A energy of these two systems. In this figure, a positive energy value represents an attractive interaction between the host (MOFs) and adsorbate (water) molecules.
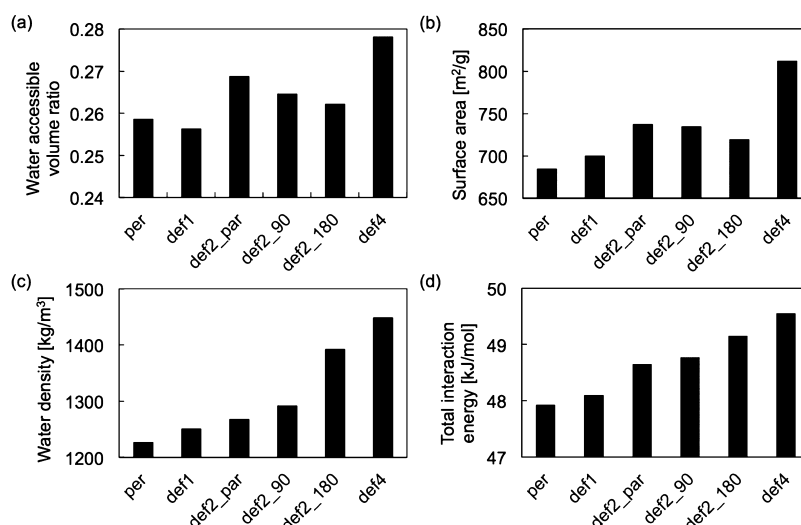
Figure 4. Structural and energetic characteristics of the perfect MOF-801 framework and defect structures. (a,b) show, respectively, the water accessible volume ratios and surface areas of MOF-801. (c,d) display the density of water and the total interaction energy of water molecules, respectively, adsorbed in MOF-801 at a relative pressure of ~93% (3500 Pa). In (d), a positive energy value represents an attractive interaction.

ranging from 0 to 25 wt %. With the introduction of defects, the Coulomb contribution to the H−A interaction energy notably increases, in particular in the low-loading region (i.e., becomes more favorable) with a slight trade-off in the vdW interaction. At a loading of less than 2 wt %, the H−A Coulomb and total interaction energies in def1 were increased by more than 3- and 2-fold, respectively, compared to that in perfect MOF-801. This enhanced interaction upon introducing structural defects can provide a stronger adsorption affinity, which has been also reflected in the computed adsorption isotherms. When the defect sites are saturated with increased loading, the H−A interaction energy (i.e., mainly from the Coulomb contribution) begins to drop and remains fairly consistent with that in the perfect structure in the high-loading region. The H−A interaction energy in the high-loading region is, however, still more favorable in def1, given a portion of the adsorbed molecules can still interact stronger with the framework defects. Similar observations can be seen for other defect structures (see Supporting Information, Figure S1).

The maximum water loading in MOFs is directly related to their performance in water adsorptive applications (e.g., a higher saturation uptake would enable a large energy density of water adsorptive heat pumps).[16] To better understand the underlying mechanism behind the varying maximum loadings for different structures shown in Figure 2, a structural analysis was performed. Figure 4a,b shows, respectively, the water-accessible volume ratio and surface area for the perfect and defective structures of MOF-801. The water-accessible volume ratio, shown in Figure 4a, was determined by investigating detailed water adsorption configurations in fully loaded MOF structures. Specifically, atomic configurations obtained from GCMC calculations at ~0.93 P/P_0 were used as starting points for NVT simulations. Approximately 8000 uncorrelated adsorption configurations were obtained from NVT simulations and superimposed. We divided the unit cell into $18 \times 18 \times 18$ voxels (i.e., the dimension of each voxel is approximately $1 \times 1 \times 1$ Å³) and analyzed if each voxel can be accessed by the oxygen atom of water molecules from the superimposed ~8000 configurations. The total water accessible volume ratio can then be calculated for each MOF structure. Using this water accessible volume is expected to provide an accurate

representation for the available space in structures that is directly accessible to water molecules. The surface area was computed by using nitrogen as a probe molecule to geometrically roll over the internal surface.[60]

Interestingly, although the accessible free volume has been generally regarded to correlate well with the maximum adsorption uptake (or the uptake in a high-pressure region),[61,62] the water-accessible volume ratio shown in Figure 4a does not correspond to the maximum loading values found in the adsorption isotherm results as given in Figure 2. The maximum loading increases as per < def1 < def2_par = def2_90 < def2_180 < def4, whereas the accessible volume instead follows the sequence of def1 < per < def2_180 < def2_90 < def2_par < def4. The accessible volume of def1 is found to be surprisingly smaller than that of perfect MOF-801 as one would intuitively anticipate that structures with defects would offer a larger available space for adsorbates. Additionally, a notable variation in the accessible volume was found in the def2 samples, although they have the same defect density. These unexpected results may be attributed to the inherently stressed structure of MOF-801. Because of the asymmetric organic ligands, an internal stress is present inside the framework and the metal clusters are slightly tilted. When a linker is removed, the force balance is disrupted, which consequently leads to a distortion of the structure (e.g., the position of metal nodes is shifted). A schematic representation of this effect can be seen in the Supporting Information, Figure S2. As a result, the removal of linkers results in a counterintuitive change in the pore volume. Similarly, it was found that the surface area, shown in Figure 4b, was also unable to explain the trend in the maximum adsorbed uptake. The surface area displays a general increase with the increased number of defects. Removing linkers will reduce the surface area contribution from the linkers, but an additional surface exposure of the metallic nodes which were originally covered by the linkers will be gained. For longer linkers, the loss of surface area from the organic linkers is more likely to outweigh the additional exposure of the metallic nodes. However, in the case of MOF-801, the linkers are small enough that the exposure of the metallic nodes is greater. For structures of the same defect density, a relatively small variation between the three studied def2 samples was observed and this can be
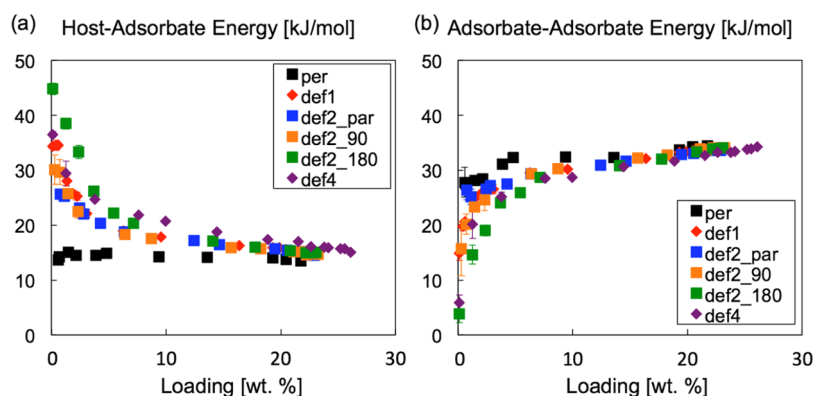
Figure 5. (a) H−A energy and the (b) A−A interaction energy as a function of loading (wt %). In this figure, a positive energy value represents an attractive interaction.

again attributed to the structural distortions. We note that the choice of using N_2 as the probe molecule would also allow the above-reported geometrical surface areas to be compared with future experimental measurements, offering a potential means to characterize the synthesized samples that possibly possess different defect densities and/or spatial configurations. Assessing the surface area of microporous MOFs using the BET method with N_2 has been the state-of-the-art approach, which also generally yields consistent surface areas as compared to that determined geometrically by rolling a probe molecule over the internal surface.[63−65]

For water adsorption in materials, as discussed above, these two commonly used geometrical features are unable to predict adsorption properties. To understand the variation in the saturated loading, we have therefore further computed the density of the adsorbed water phase, shown in Figure 4c, by the total water-accessible volume and the maximum loading at a ∼93% relative pressure for each material. Surprisingly, the density of adsorbed water in different materials was found to differ by as much as 20%. The corresponding total interaction energies of adsorbed water molecules were also computed as given in Figure 4d. Although comparing the density of the adsorbed water (Figure 4c) to its total interaction energy (Figure 4d), a strong positive correlation was observed, indicating that the enhancement in the interaction energy of water molecules due to the introduction of defects has led to a much denser water phase. With such energetic information together with the geometric characteristics at our disposal, the trend in the saturation adsorption update can be now well-explained. For instance, although the structural distortion of def1 has led to a smaller total available water-accessible volume compared to the perfect crystal, its enhanced interaction energies with a denser adsorbed phase resulted in an overall higher maximum uptake. Our results suggest that an optimization of the surface chemistry providing a better stabilization to the adsorbed water phase may be a key to enhance the adsorption capacity. At this point, it is important to also discuss the profound effects of the spatial defect configurations on their water adsorption characteristics. From the adsorption energies of water in def2 structures with different arrangements, the def2_180 shows the largest total interaction whereas def2_par and def2_90 possess lower and relatively similar total interaction energies. We found that with the specific spatial defect arrangement in def2_180 (same in def4), large and continuous hydrophilic defect channels along the [110] direction can be formed. Such hydrophilic channels

provide strong interactions with water molecules as well as facilitate the clustering of water molecules, creating a more condensed phase compared to other defect configurations. A schematic presentation of the hydrophilic channels can be found in Figure S3 of the Supporting Information.

Figure 5 shows the interaction energies of water adsorbed in each structure as a function of water uptake. The total interaction energies are decomposed into two components: H−A and adsorbate−adsorbate (denoted as A−A, interactions between water and water molecules). In general, as mentioned previously, all defect samples show a notably more favorable H−A energy compared to the perfect structure at a low loading (i.e., low-pressure region), indicating strong interactions from the more hydrophilic nature of the structures with defects. Among all samples, def2_180 offers the strongest interaction energy between the host material and the adsorbate molecule followed by def4. At a low pressure, one would expect that the defect structures with stronger H−A interaction would simply exhibit greater adsorption.[66,67] Interestingly, comparing the uptake at low pressures from the isotherms and the interaction energy results, it can be seen that the H−A energy cannot explain fully the observed adsorptive behavior. This may be attributed to the fact that, even in the low-pressure region, the A−A interaction also contributes significantly to the adsorption behavior. As shown in Figure 5, the A−A interaction energy in def2_par at a low pressure is more favorable than that in, for instance, def2_180. A−A interaction energies are primarily determined by the relative adsorption configurations between adjacent adsorbed molecules, depending on a variety of factors including, but not limited to, surface chemistry and pore confinement. A detailed investigation to understand the adsorption configurations of water in structures with defects and their configurational changes upon adsorption will be an important subject of future study.

Finally, the evolution of the water adsorption in MOF-801 as a function of relative pressures was explored at an atomic level with the water density contour plots for def1 and def4 structures shown in Figure 6. The density of water molecules is examined by dividing the MOF structure into four areas along the z-axis (i.e., crystallographic c-direction). The thickness of each cross-section is 4.46 Å, 1/4 of the lattice dimension of the unit cell. In the def1 structure, at a low relative pressure of 0−27%, water molecules as expected first get adsorbed near the defect sites because of the strong H−A interactions, forming local water clusters around the hydrogenated oxygen in the metal cluster. With the local water clusters formed near the
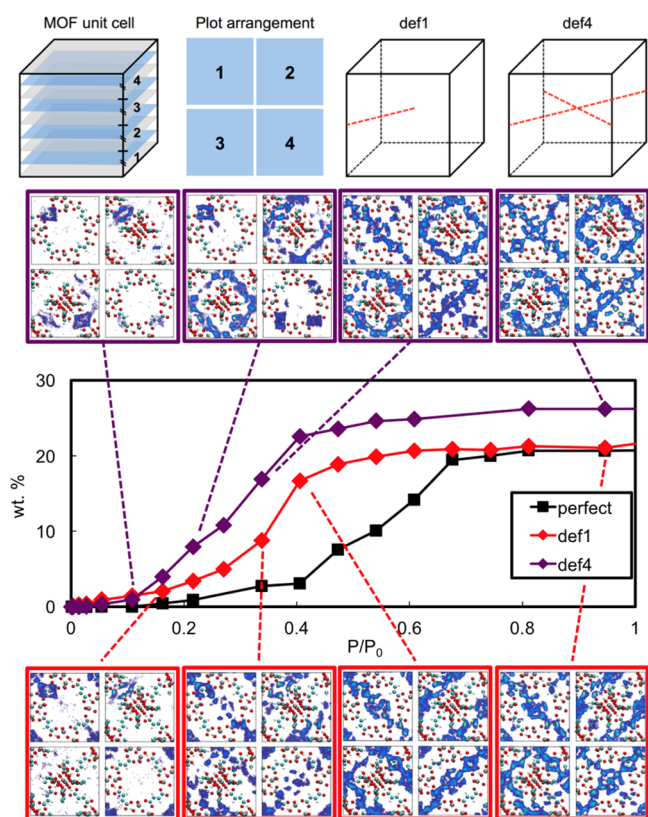
Figure 6. Water density plots in def1 and def4 structures at different adsorption loadings (wt %). The cross-sectional cut and the layout of the density contours plots are schematically shown in the upper panel of the figure. The position of missing linkers in def1 and def4 structures is also highlighted in red dashed lines. The water density plots in the perfect MOF-801 structure can be seen in the Supporting Information Figure S4.

defects, they further facilitate water adsorption at a lower relative pressure and lead to a sharper increase in uptake at a lower relative pressure as compared to that in the perfect crystal (see Supporting Information Figure S4 for the evolution of water adsorption in the perfect MOF-801 structure). Water molecules are preferentially adsorbed in tetrahedral channels along the ⟨110⟩ direction, and not all channels have equal water densities. This unequal water adsorption can be attributed to the heterogeneous energy surface because of (a) the presence of defects and (b) the position of the hydroxyl groups in the metal clusters (i.e., $Zr_6O_4(OH)_4$). When the adsorption gradually reaches full saturation, the remaining free pore volumes become filled. Similarly, for the def4 case, in the low-pressure region below 10% relative pressure, water molecules are also adsorbed first near the defect sites. However, the pores, specifically the preferential tetrahedral channels along the ⟨110⟩, are much more quickly filled up, and the condensation starts to occur at a lower relative pressure of 10%. In the def4 structure, all defects are placed along the preferential adsorption direction (i.e., ⟨110⟩ direction, see Figure S3 of the Supporting Information and the discussion above), resulting in large and continuous hydrophilic channels to allow a more uniform water adsorption along the defect sites and facilitate a rapid water uptake. It should be noted again that there exists a collective effect for the water adsorption in def4 as both H−A and A−A interaction energies contribute substan-

tially to the adsorption. Same as that in def1, all pores are eventually filled up at a higher pressure.

CONCLUSIONS

The water adsorption properties of MOF-801 were investigated in this study. Perfect MOF-801 and MOF-801 structures with different defect configurations were examined to gain a comprehensive understanding of how the density and spatial arrangement of defects affect the water adsorption properties. Our work has shown that the experimental adsorptive behaviors can be explained through the presence of defects with the actual structure believed to possess a high defect density. With the increased number of missing-linker defects, MOF structures possess more hydrophilic characteristics (i.e., stronger initial adsorption strength and steep uptake occurring at a lower pressure). This can be mainly attributed to the increased H−A Coulomb interactions inside the defect structures. It was also found that the interaction energies of the adsorbed water inside confinements play an important role in determining their saturation adsorption uptake. Although the total free pore volume that is available to adsorbates has been generally regarded to correlate with the saturation uptake of adsorbates, varying degrees of energy stabilization for adsorbed water can result in a notable difference in its density (i.e., a difference as high as 20% was observed). This result suggests that, for applications such as water harvesting and heat pumps using MOFs, optimizing the surface chemistry by controlling defects via different synthesis approaches and/or tuning ligands may largely improve their storage performance. Additionally, our calculations indicate that, unlike other gases such as CO_2 and N_2, the adsorptive behavior of water in the low-pressure region depends not only on the H−A interactions but also on the A−A interactions. Finally, a preferential water condensation was identified in the ⟨110⟩ directions of MOF-801, along the tetrahedral pore sites. When defects exist in this direction (e.g., def4 and def2_180), stronger adsorptive behavior can be realized. This highlights the importance of the spatial configurations of defects in the water adsorption properties. It should be noted, however, that the spatial arrangement of defects and the defect types were not exhaustively explored in this study (e.g., only one defect arrangement was studied for the defect density of 1/6 and only missing-linker defects were considered), and an extensive investigation of these effects can be an important subject of future studies. Overall, this work has illustrated the role of defects and offers a microscopic picture of their effects on the adsorption properties of water in MOFs.

ASSOCIATED CONTENT

ⓢ Supporting Information

The Supporting Information is available free of charge on the ACS Publications website at DOI: 10.1021/acs.jpcc.8b00014.

> Additional figures referred in the main article and the coordinate files of all studied structures including the detailed energy contributions to the interactions between water molecules and MOF frameworks in all studied structures, schematic illustrations of the structural changes due to the missing linkers and the hydrophilic channels observed in def2_180 and def4 structures, water density plots of the perfect MOF-801 structure at different loadings, and structure information (PDF)

■ AUTHOR INFORMATION

Corresponding Authors
*E-mail: lin.2645@osu.edu (L.-C.L.).
*E-mail: jcg@mit.edu (J.C.G.).

ORCID
Li-Chiang Lin: 0000-0002-2821-9501

Author Contributions
This study was developed and completed through contributions by all authors, and all authors have given approval to the final version of the manuscript.

Notes
The authors declare no competing financial interest.

■ ABBREVIATIONS

H−A, host−adsorbate; A−A, adsorbate−adsorbate

■ REFERENCES

(1) Li, H. L.; Eddaoudi, M. M.; O'Keeffe, M.; Yaghi, O. M. Design and Synthesis of an Exceptionally Stable and Highly Porous Metal-Organic Framework. *Nature* **1999**, *402*, 276−279.

(2) Lee, J.; Farha, O. K.; Roberts, J.; Scheidt, K. A.; Nguyen, S. T.; Hupp, J. T. Metal-Organic Framework Materials as Catalysts. *Chem. Soc. Rev.* **2009**, *38*, 1450−1459.

(3) Kreno, L. E.; Leong, K.; Farha, O. K.; Allendorf, M.; Van Duyne, R. P.; Hupp, J. T. Metal−Organic Framework Materials as Chemical Sensors. *Chem. Rev.* **2012**, *112*, 1105−1125.

(4) Stock, N.; Biswas, S. Synthesis of Metal-Organic Frameworks (MOFs): Routes to Various MOF Topologies, Morphologies, and Composites. *Chem. Rev.* **2012**, *112*, 933−969.

(5) Li, J.-R.; Kuppler, R. J.; Zhou, H.-C. Selective Gas Adsorption and Separation in Metal-Organic Frameworks. *Chem. Soc. Rev.* **2009**, *38*, 1477−1504.

(6) Furukawa, H.; Cordova, K. E.; O'Keeffe, M.; Yaghi, O. M. The Chemistry and Applications of Metal-Organic Frameworks. *Science* **2013**, *341*, 1230444.

(7) Farha, O. K.; Eryazici, I.; Jeong, N. C.; Hauser, B. G.; Wilmer, C. E.; Sarjeant, A. A.; Snurr, R. Q.; Nguyen, S. T.; Yazaydın, A. Ö.; Hupp, J. T. Metal−Organic Framework Materials with Ultrahigh Surface Areas: Is the Sky the Limit? *J. Am. Chem. Soc.* **2012**, *134*, 15016−15021.

(8) Huck, J. M.; Lin, L.-C.; Berger, A. H.; Shahrak, M. N.; Martin, R. L.; Bhown, A. S.; Haranczyk, M.; Reuter, K.; Smit, B. Evaluating Different Classes of Porous Materials for Carbon Capture. *Energy Environ. Sci.* **2014**, *7*, 4132−4146.

(9) Kim, J.; Lin, L.-C.; Martin, R. L.; Swisher, J. A.; Haranczyk, M.; Smit, B. Large-Scale Computational Screening of Zeolites for Ethane/Ethene Separation. *Langmuir* **2012**, *28*, 11914−11919.

(10) D'Alessandro, D. M.; Smit, B.; Long, J. R. Carbon Dioxide Capture: Prospects for New Materials. *Angew. Chem., Int. Ed.* **2010**, *49*, 6058−6082.

(11) Kim, H.; Yang, S.; Rao, S. R.; Narayanan, S.; Kapustin, E. A.; Furukawa, H.; Umans, A. S.; Yaghi, O. M.; Wang, E. N. Water Harvesting from Air with Metal-Organic Frameworks Powered by Natural Sunlight. *Science* **2017**, *356*, 430−434.

(12) Henninger, S. K.; Habib, H. A.; Janiak, C. MOFs as Adsorbents for Low Temperature Heating and Cooling Applications. *J. Am. Chem. Soc.* **2009**, *131*, 2776−2777.

(13) Ehrenmann, J.; Henninger, S. K.; Janiak, C. Water Adsorption Characteristics of MIL-101 for Heat-Transformation Applications of MOFs. *Eur. J. Inorg. Chem.* **2011**, *471−474*.

(14) Kim, H.; Cho, H. J.; Narayanan, S.; Yang, S.; Furukawa, H.; Schiffres, S.; Li, X.; Zhang, Y.-B.; Jiang, J.; Yaghi, O. M.; et al. Characterization of Adsorption Enthalpy of Novel Water-Stable Zeolites and Metal-Organic Frameworks. *Sci. Rep.* **2016**, *6*, 19097.

(15) de Lange, M. F.; van Velzen, B. L.; Ottevanger, C. P.; Verouden, K. J. F. M.; Lin, L.-C.; Vlugt, T. J. H.; Gascon, J.; Kapteijn, F. Metal−Organic Frameworks in Adsorption-Driven Heat Pumps: The Potential of Alcohols as Working Fluids. *Langmuir* **2015**, *31*, 12783−12796.

(16) de Lange, M. F.; Verouden, K. J. F. M.; Vlugt, T. J. H.; Gascon, J.; Kapteijn, F. Adsorption-Driven Heat Pumps: The Potential of Metal−Organic Frameworks. *Chem. Rev.* **2015**, *115*, 12205−12250.

(17) Fang, Z.; Bueken, B.; De Vos, D. E.; Fischer, R. A. Defect-Engineered Metal−Organic Frameworks. *Angew. Chem., Int. Ed.* **2015**, *54*, 7234−7254.

(18) Bai, Y.; Dou, Y.; Xie, L.-H.; Rutledge, W.; Li, J.-R.; Zhou, H.-C. Zr-Based Metal-Organic Frameworks: Design, Synthesis, Structure, and Applications. *Chem. Soc. Rev.* **2016**, *45*, 2327−2367.

(19) Chong, S.; Thiele, G.; Kim, J. Excavating Hidden Adsorption Sites in Metal-Organic Frameworks Using Rational Defect Engineering. *Nat. Commun.* **2017**, *8*, 1539.

(20) Valenzano, L.; Civalleri, B.; Chavan, S.; Bordiga, S.; Nilsen, M. H.; Jakobsen, S.; Lillerud, K. P.; Lamberti, C. Disclosing the Complex Structure of UiO-66 Metal Organic Framework: A Synergic Combination of Experiment and Theory. *Chem. Mater.* **2011**, *23*, 1700−1718.

(21) Cliffe, M. J.; Wan, W.; Zou, X.; Chater, P. A.; Kleppe, A. K.; Tucker, M. G.; Wilhelm, H.; Funnell, N. P.; Coudert, F.-X.; Goodwin, A. L. Correlated Defect Nanoregions in a Metal−organic Framework. *Nat. Commun.* **2014**, *5*, 4176.

(22) Shearer, G. C.; Chavan, S.; Ethiraj, J.; Vitillo, J. G.; Svelle, S.; Olsbye, U.; Lamberti, C.; Bordiga, S.; Lillerud, K. P. Tuned to Perfection: Ironing Out the Defects in Metal−Organic Framework UiO-66. *Chem. Mater.* **2014**, *26*, 4068−4071.

(23) Taylor, J. M.; Dekura, S.; Ikeda, R.; Kitagawa, H. Defect Control To Enhance Proton Conductivity in a Metal−Organic Framework. *Chem. Mater.* **2015**, *27*, 2286−2289.

(24) Wu, H.; Chua, Y. S.; Krungleviciute, V.; Tyagi, M.; Chen, P.; Yildirim, T.; Zhou, W. Unusual and Highly Tunable Missing-Linker Defects in Zirconium Metal−Organic Framework UiO-66 and Their Important Effects on Gas Adsorption. *J. Am. Chem. Soc.* **2013**, *135*, 10525−10532.

(25) Cavka, J. H.; Jakobsen, S.; Olsbye, U.; Guillou, N.; Lamberti, C.; Bordiga, S.; Lillerud, K. P. A New Zirconium Inorganic Building Brick Forming Metal Organic Frameworks with Exceptional Stability. *J. Am. Chem. Soc.* **2008**, *130*, 13850−13851.

(26) Dissegna, S.; Hardian, R.; Epp, K.; Kieslich, G.; Coulet, M.-V.; Llewellyn, P.; Fischer, R. A. Using Water Adsorption Measurements to Access the Chemistry of Defects in the Metal-Organic Framework UiO-66. *CrystEngComm* **2017**, *19*, 4137−4141.

(27) Ghosh, P.; Colón, Y. J.; Snurr, R. Q. Water Adsorption in UiO-66: The Importance of Defects. *Chem. Commun.* **2014**, *50*, 11329−11331.

(28) Liang, W.; Coghlan, C. J.; Ragon, F.; Rubio-Martinez, M.; D'Alessandro, D. M.; Babarao, R. Defect Engineering of UiO-66 for CO_2 and H_2O Uptake—a Combined Experimental and Simulation Study. *Dalton Trans.* **2016**, *45*, 4496−4500.

(29) Wißmann, G.; Schaate, A.; Lilienthal, S.; Bremer, I.; Schneider, A. M.; Behrens, P. Modulated Synthesis of Zr-Fumarate MOF. *Microporous Mesoporous Mater.* **2012**, *152*, 64−70.

(30) Furukawa, H.; Gándara, F.; Zhang, Y.-B.; Jiang, J.; Queen, W. L.; Hudson, M. R.; Yaghi, O. M. Water Adsorption in Porous Metal−

Organic Frameworks and Related Materials. *J. Am. Chem. Soc.* **2014**, *136*, 4369−4381.

(31) Kresse, G.; Furthmüller, J. Efficient Iterative Schemes for Ab Initio Total-Energy Calculations Using a Plane-Wave Basis Set. *Phys. Rev. B: Condens. Matter Mater. Phys.* **1996**, *54*, 11169−11186.

(32) Kresse, G.; Hafner, J. Ab Initio Molecular Dynamics for Liquid Metals. *Phys. Rev. B: Condens. Matter Mater. Phys.* **1993**, *47*, 558−561.

(33) Kresse, G.; Hafner, J. Ab Initio Molecular-Dynamics Simulation of the Liquid-Metal−Amorphous-Semiconductor Transition in Germanium. *Phys. Rev. B: Condens. Matter Mater. Phys.* **1994**, *49*, 14251−14269.

(34) Blöchl, P. E. Projector Augmented-Wave Method. *Phys. Rev. B: Condens. Matter Mater. Phys.* **1994**, *50*, 17953−17979.

(35) Kresse, G.; Joubert, D. From Ultrasoft Pseudopotentials to the Projector Augmented-Wave Method. *Phys. Rev. B: Condens. Matter Mater. Phys.* **1999**, *59*, 1758−1775.

(36) Perdew, J. P.; Burke, K.; Ernzerhof, M. Generalized Gradient Approximation Made Simple. *Phys. Rev. Lett.* **1996**, *77*, 3865−3868.

(37) Perdew, J. P.; Burke, K.; Ernzerhof, M. Generalized Gradient Approximation Made Simple. *Phys. Rev. Lett.* **1997**, *78*, 1396.

(38) Dubbeldam, D.; Calero, S.; Ellis, D. E.; Snurr, R. Q. RASPA: Molecular Simulation Software for Adsorption and Diffusion in Flexible Nanoporous Materials. *Mol. Simul.* **2016**, *42*, 81−101.

(39) Frenkel, D.; Smit, B. *Understanding Molecular Simulation*, 2nd ed.; Academic Press: San Diego, 2002.

(40) Mayo, S. L.; Olafson, B. D.; Goddard, W. A. DREIDING: A Generic Force Field for Molecular Simulations. *J. Phys. Chem.* **1990**, *94*, 8897−8909.

(41) Rappe, A. K.; Casewit, C. J.; Colwell, K. S.; Goddard, W. A.; Skiff, W. M. UFF, a Full Periodic Table Force Field for Molecular Mechanics and Molecular Dynamics Simulations. *J. Am. Chem. Soc.* **1992**, *114*, 10024−10035.

(42) Campañá, C.; Mussard, B.; Woo, T. K. Electrostatic Potential Derived Atomic Charges for Periodic Systems Using a Modified Error Functional. *J. Chem. Theory Comput.* **2009**, *5*, 2866−2878.

(43) Horn, H. W.; Swope, W. C.; Pitera, J. W.; Madura, J. D.; Dick, T. J.; Hura, G. L.; Head-Gordon, T. Development of an Improved Four-Site Water Model for Biomolecular Simulations: TIP4P-Ew. *J. Chem. Phys.* **2004**, *120*, 9665−9678.

(44) Horn, H. W.; Swope, W. C.; Pitera, J. W. Characterization of the TIP4P-Ew Water Model: Vapor Pressure and Boiling Point. *J. Chem. Phys.* **2005**, *123*, 194504.

(45) Lin, L.-C.; Lee, K.; Gagliardi, L.; Neaton, J. B.; Smit, B. Force-Field Development from Electronic Structure Calculations with Periodic Boundary Conditions: Applications to Gaseous Adsorption and Transport in Metal-Organic Frameworks. *J. Chem. Theory Comput.* **2014**, *10*, 1477−1488.

(46) Yang, D.-A.; Cho, H.-Y.; Kim, J.; Yang, S.-T.; Ahn, W.-S. CO2 Capture and Conversion Using Mg-MOF-74 Prepared by a Sonochemical Method. *Energy Environ. Sci.* **2012**, *5*, 6465−6473.

(47) Schoenecker, P. M.; Carson, C. G.; Jasuja, H.; Flemming, C. J. J.; Walton, K. S. Effect of Water Adsorption on Retention of Structure and Surface Area of Metal−Organic Frameworks. *Ind. Eng. Chem. Res.* **2012**, *51*, 6513−6519.

(48) Grant Glover, T.; Peterson, G. W.; Schindler, B. J.; Britt, D.; Yaghi, O. MOF-74 Building Unit Has a Direct Impact on Toxic Gas Adsorption. *Chem. Eng. Sci.* **2011**, *66*, 163−170.

(49) Jiang, Z.-R.; Wang, H.; Hu, Y.; Lu, J.; Jiang, H.-L. Polar Group and Defect Engineering in a Metal−Organic Framework: Synergistic Promotion of Carbon Dioxide Sorption and Conversion. *ChemSusChem* **2015**, *8*, 878−885.

(50) Vermoortele, F.; Bueken, B.; Le Bars, G.; Van de Voorde, B.; Vandichel, M.; Houthoofd, K.; Vimont, A.; Daturi, M.; Waroquier, M.; Van Speybroeck, V.; et al. Synthesis Modulation as a Tool To Increase the Catalytic Activity of Metal−Organic Frameworks: The Unique Case of UiO-66(Zr). *J. Am. Chem. Soc.* **2013**, *135*, 11465−11468.

(51) Vandichel, M.; Hajek, J.; Vermoortele, F.; Waroquier, M.; De Vos, D. E.; Van Speybroeck, V. Active Site Engineering in UiO-66 Type Metal-Organic Frameworks by Intentional Creation of Defects: A Theoretical Rationalization. *CrystEngComm* **2015**, *17*, 395−406.

(52) Dzubak, A. L.; Lin, L.-C.; Kim, J.; Swisher, J. A.; Poloni, R.; Maximoff, S. N.; Smit, B.; Gagliardi, L. Ab Initio Carbon Capture in Open-Site Metal−organic Frameworks. *Nat. Chem.* **2012**, *4*, 810−816.

(53) Fang, H.; Kamakoti, P.; Zang, J.; Cundy, S.; Paur, C.; Ravikovitch, P. I.; Sholl, D. S. Prediction of CO2 Adsorption Properties in Zeolites Using Force Fields Derived from Periodic Dispersion-Corrected DFT Calculations. *J. Phys. Chem. C* **2012**, *116*, 10692−10701.

(54) Borycz, J.; Lin, L.-C.; Bloch, E. D.; Kim, J.; Dzubak, A. L.; Maurice, R.; Semrouni, D.; Lee, K.; Smit, B.; Gagliardi, L. CO2 Adsorption in Fe2(dobdc): A Classical Force Field Parameterized from Quantum Mechanical Calculations. *J. Phys. Chem. C* **2014**, *118*, 12230−12240.

(55) Rudenko, A. N.; Bendt, S.; Keil, F. J. Multiscale Modeling of Water in Mg-MOF-74: From Electronic Structure Calculations to Adsorption Isotherms. *J. Phys. Chem. C* **2014**, *118*, 16218−16227.

(56) Zang, J.; Nair, S.; Sholl, D. S. Prediction of Water Adsorption in Copper-Based Metal−Organic Frameworks Using Force Fields Derived from Dispersion-Corrected DFT Calculations. *J. Phys. Chem. C* **2013**, *117*, 7519−7525.

(57) Mercado, R.; Vlaisavljevich, B.; Lin, L.-C.; Lee, K.; Lee, Y.; Mason, J. A.; Xiao, D. J.; Gonzalez, M. I.; Kapelewski, M. T.; Neaton, J. B.; et al. Force Field Development from Periodic Density Functional Theory Calculations for Gas Separation Applications Using Metal−Organic Frameworks. *J. Phys. Chem. C* **2016**, *120*, 12590−12604.

(58) Shi, W.; Maginn, E. J. Continuous Fractional Component Monte Carlo: An Adaptive Biasing Method for Open System Atomistic Simulations. *J. Chem. Theory Comput.* **2007**, *3*, 1451−1463.

(59) Zhang, H.; Snurr, R. Q. Computational Study of Water Adsorption in the Hydrophobic Metal−Organic Framework ZIF-8: Adsorption Mechanism and Acceleration of the Simulations. *J. Phys. Chem. C* **2017**, *121*, 24000−24010.

(60) Düren, T.; Millange, F.; Férey, G.; Walton, K. S.; Snurr, R. Q. Calculating Geometric Surface Areas as a Characterization Tool for Metal−Organic Frameworks. *J. Phys. Chem. C* **2007**, *111*, 15350−15356.

(61) Wilmer, C. E.; Leaf, M.; Lee, C. Y.; Farha, O. K.; Hauser, B. G.; Hupp, J. T.; Snurr, R. Q. Large-Scale Screening of Hypothetical Metal−organic Frameworks. *Nat. Chem.* **2011**, *4*, 83−89.

(62) Martin, R. L.; Lin, L.-C.; Jariwala, K.; Smit, B.; Haranczyk, M. Mail-Order Metal−Organic Frameworks (MOFs): Designing Isoreticular MOF-5 Analogues Comprising Commercially Available Organic Molecules. *J. Phys. Chem. C* **2013**, *117*, 12159−12167.

(63) Walton, K. S.; Snurr, R. Q. Applicability of the BET Method for Determining Surface Areas of Microporous Metal-Organic Frameworks. *J. Am. Chem. Soc.* **2007**, *129*, 8552−8556.

(64) Gómez-Gualdrón, D. A.; Moghadam, P. Z.; Hupp, J. T.; Farha, O. K.; Snurr, R. Q. Application of Consistency Criteria To Calculate BET Areas of Micro- And Mesoporous Metal−Organic Frameworks. *J. Am. Chem. Soc.* **2016**, *138*, 215−224.

(65) de Lange, M. F.; Lin, L.-C.; Gascon, J.; Vlugt, T. J. H.; Kapteijn, F. Assessing the Surface Area of Porous Solids: Limitations, Probe Molecules, and Methods. *Langmuir* **2016**, *32*, 12664−12675.

(66) Lin, L.-C.; Berger, A. H.; Martin, R. L.; Kim, J.; Swisher, J. A.; Jariwala, K.; Rycroft, C. H.; Bhown, A. S.; Deem, M. W.; Haranczyk, M.; et al. In Silico Screening of Carbon-Capture Materials. *Nat. Mater.* **2012**, *11*, 633−641.

(67) Wilmer, C. E.; Farha, O. K.; Bae, Y.-S.; Hupp, J. T.; Snurr, R. Q. Structure−property Relationships of Porous Materials for Carbon Dioxide Separation and Capture. *Energy Environ. Sci.* **2012**, *5*, 9849−9856.

(68) Ohio Supercomputer Center. http://osc.edu/ark:/19495/f5s1ph73. accessed Feb 16, 2018.